

The Effects of HCN and KLT Ion Channels on Adaptation and Refractoriness in a Stochastic Auditory Nerve Model

Mohamed H. Negm, *Student Member, IEEE*, and Ian C. Bruce*, *Senior Member, IEEE*

Abstract—An accurate model of auditory nerve fibers (ANFs) may assist in developing improved cochlear implant (CI) stimulation strategies. Previous studies have shown that the original Hodgkin–Huxley (HH) model may be better at describing nodes of Ranvier in ANFs than models for other mammalian axon types. However, the HH model is still unable to explain a number of phenomena observed in auditory nerve responses to CI stimulation such as adaptation to high-rate stimulation and the time course of relative refractoriness. Recent physiological investigations of ANFs have shown the presence of a number of ion channel types not considered in the previous modeling studies, including low-threshold potassium (KLT) channels and hyperpolarization-activated cation (HCN) channels. In this paper, we investigate inclusion of these ion channel types in a stochastic HH model of a single node of Ranvier. Simulation results for pulse trains with rates of 200, 800, and 2000 pulse/s suggests that both the KLT channels and HCN channels can produce adaptation in the spike rate. However, the adaptation due to KLT is restricted to higher stimulation rates, whereas the adaptation due to HCN is observed across all stimulation rates. Additionally, using pulse pairs it was found that KLT increased both the absolute and the relative refractory periods. HCN on its own increased just the relative refractory period, but produced a synergistic increase in the absolute refractory period when combined with KLT. Together these results argue strongly for the need to consider HCN and KLT channels when studying CI stimulation of ANFs.

Index Terms—Adaptation, auditory nerve fibers (ANFs), cochlear implants (CIs), refractoriness.

I. INTRODUCTION

COCHLEAR implants (CIs) are prosthetic devices used to restore hearing for severely deaf individuals. CIs stimulate the auditory nerve fibers (ANFs) by applying electrical current pulses via an electrode array inserted inside the cochlea. From a relatively early stage in CI development, there has been an interest in using very high pulse rates (e.g., [1]), but speech perception does not necessarily improve at higher stimulation rates (e.g., [2]). The variability across patients in the optimal stimulation rate motivates a better understanding of the neurophys-

iological mechanisms underlying ANF responses to high-rate electrical stimulation.

Analyses of the *refractory* properties of feline ANFs for electrical stimulation have shown that on average they have very fast refractory recovery compared to other types of neurons [3]–[5]. However, there is a substantial amount of variability in refractory periods between different ANFs, and a large subset of ANFs exhibit an extended period of relative refractoriness lasting to at least 4 ms (see [3, Fig. 8] and [4, Fig. 7]). Extended refractoriness in a subpopulation of ANFs has also been observed in human CI subjects [6], [7]. Stimulation with pairs of pulses has also demonstrated *facilitation* (also referred to as summation or sensitization) for spike generation in response to the second pulse in cases, where the first pulse did not elicit a spike [3], [5], [8]. Facilitation time constants for feline ANFs are in the order of 100 to 400 μ s and are partly dependent on the site of spike generation [5]. Evidence of facilitation has also been observed in human CI users [6] and in guinea pig ANFs for pulse-train stimulation [9]. After the period of facilitation is over for a subthreshold first pulse, a period of *accommodation* (also referred to as subthreshold masking or desensitization) can be observed in some ANFs [8], during which the threshold current for the second pulse is *increased* relative to the first-pulse threshold current, in contrast to the *decrease* that occurs during the facilitation period. Accommodation has also been observed for high-rate pulse trains [8], [10]. In addition, ongoing spiking from high-rate pulse trains produces spike-rate *adaptation* in ANFs [10]–[13], although for a continuous pulse train with a fixed amplitude it is difficult to disentangle the effects of refractoriness, facilitation, accommodation, and adaptation.

Several computational models have been developed to describe ANF behavior. Many of these have been based on the deterministic Hodgkin–Huxley (HH) model [14]. In their extensive study, [14] modeled the fast sodium and delayed rectified potassium ion channels of the squid giant axon at 6.3 °C. Cartee showed that the temperature-adjusted HH model may be a better model for ANFs than alternative models developed for other myelinated nerve fibers [15]. However, Verveen and Derksen reported significant stochastic fluctuations in membrane potential from myelinated nerve fibers of a frog [16], which suggested that the deterministic HH equations may provide an impoverished description of real neural membranes. The magnitude of these fluctuations in membrane potential is inversely proportional to node diameter [17]. An average diameter of an axon at a node of Ranvier for a mammalian ANF ranges between 2 and 4 μ m, and many nodes are even smaller [18].

Manuscript received March 13, 2014; revised May 5, 2014; accepted May 22, 2014. Date of publication May 29, 2014; date of current version October 16, 2014. This work was supported by NSERC Discovery Grant 261736, the Barber–Gennum Chair Endowment, and the Faculty of Engineering at McMaster University. *Asterisk indicates corresponding author.*

M. H. Negm is with the Department of Electrical and Computer Engineering, McMaster University, Hamilton, ON L8S 4K1, Canada (e-mail: negmmh@mcmaster.ca).

*I. C. Bruce is with the Department of Electrical and Computer Engineering, McMaster University, Hamilton, ON L8S 4K1, Canada (e-mail: ibruce@ieee.org).

Digital Object Identifier 10.1109/TBME.2014.2327055

Therefore, the noise activity in membrane potential becomes more significant when dealing with ANFs. Bruce *et al.* subsequently showed that stochastic models for ANFs better predict physiological responses and psychophysical performance [18]. Therefore, recent versions of HH-based ANF models have typically used stochastic ion channel implementations [10], [19]–[28]. However, the refractoriness, facilitation, accommodation, and adaptation properties of AN responses to CI stimulation are still not completely described by any of these models.

A number of physiological studies have shown the presence of different ion channel types in cultured spiral ganglion neuron (SGN) soma¹ [29]–[33], other than the fast voltage-gated sodium (Na_v) and delayed rectifier potassium (Kv) channels of the HH model. These physiological experiments suggest that the diversity in ion channel types and distribution affect the firing properties and participate in the signal coding and transformation in the auditory periphery [30], [33]. Among these channels are voltage-gated hyperpolarization-activated cation (HCN) channels and voltage-gated low-threshold potassium (KLT) channels that permit the passage of I_h and I_{KLT} currents, respectively. I_h is an inward rectifier current that is observed in different regions across the lower auditory system, such as the SGN soma [30], [31], [34], ANF peripheral terminals [34], a variety of ventral cochlear nucleus (VCN) neurons [35]–[38], the medial superior olive (MSO) neurons [39], and lateral lemniscus [40]. I_h is characterized by being a mixed cation current (channels are permeable to both sodium and potassium ions), the reversal potential is more positive than the resting membrane potential, and it has slow activation/deactivation time constants [30]. I_h contributes also in determining the resting potential [38], at which I_h is partially activated, and controls the spontaneous and evoked firing rates. I_h has heterogeneous activation characteristics [30], i.e., reversal potential, half-maximal voltage $V_{1/2}$, and slope factor k that are attributed to endogenous regulatory mechanisms that differ from one neuron to another in the spiral ganglion.

I_{KLT} tends to colocalize with I_h , being found in the SGN soma [32], [33], VCN cells [36], [41], and MSO neurons [39]. KLT channels may also be present in ANF central-axon nodes of Ranvier [42], where HCN channels are not thought to be expressed. Like I_h , I_{KLT} is partially activated at rest and works with the high-threshold Kv channels in repolarizing the membrane, shortening the duration of synaptic potentials and action potentials [33], [36]. I_{KLT} has relatively slow dynamics, such that it produces adaptation in spiking to sustained current injections [32], [33], [43]. It exhibits variability in the amount slow inactivation, with an average of around 50% inactivation [36].

The characteristics of I_h and I_{KLT} suggest that these two channel types could play an important role in determining the temporal response properties of ANFs to electrical stimulation from CIs. In this paper, we present a model for a patch of membrane, at the node of Ranvier of an ANF. Four stochastic

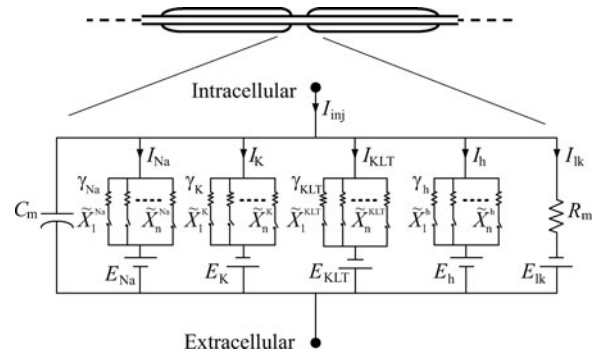


Fig. 1. Model for a patch of membrane at a node of Ranvier: C_m , R_m , γ_x , E_x are the membrane capacitance, membrane leakage resistance, single channel conductances, and reversal potentials, respectively. X_i^x are the stochastic single-channel states (open or closed). E_{lk} is the leakage potential.

ion channels are modeled. The two channels 1) KLT and 2) HCN channels are incorporated in the model together with the classical fast Na_v and delayed rectifier Kv of the HH model. We utilized the channel models of [36], based on the thoroughly characterized channel properties from VCN cells [44], [45]. In a preliminary study with an early version of this model, we showed that these channels can effect single-pulse response properties, particularly for long-duration pulses [46]. In this paper, our analysis focuses on the adaptation and refractory properties of the model. A preliminary version of parts of this work has been reported [47]. The simulation results suggest that I_h and I_{KLT} currents can have a strong effect on the intrinsic response properties of ANFs to CI stimulation and should, therefore, be incorporated in computational models of ANFs.

II. METHODS

A. Membrane Model

A single node of Ranvier in a mammalian ANF was modeled. The node consisted of four voltage-gated ion channel types, which are: 1) fast sodium (Na_v) channels; 2) delayed-rectifier potassium (Kv) channels; 3) KLT channels; and 4) HCN channels that controlled the passage of I_{Na} , I_K , I_{KLT} , and I_h currents, respectively. A passive leakage channel was included (that produced the I_{lk} current) with the reversal potential E_{lk} adjusted for each version of the model to maintain a constant resting membrane potential at -78 mV. The equivalent circuit of the model is shown in Fig. 1 and the model parameters are given in Table I. The single channel conductances and temperature scaling coefficients for the HCN and KLT channels in ANFs have not yet been published, so values were chosen based on advice from research groups who study these channels in auditory neurons. Likewise, the channel densities are not known for these channels, so plausible values that give reasonable behavior were chosen for the default channel counts. The effects of the channel counts on the model response properties were investigated in a sensitivity analysis.

¹The terminology of ANF and SGN are used somewhat interchangeably in the literature. However, in this study, we will mainly use SGN when referring to the cell body (or soma) and ANF when referring to the peripheral or central processes (or axons).

TABLE I
SUMMARY OF PARAMETERS FOR THE MEMBRANE MODEL

Parameter	Symbol	Value	Unit	Ref.
Nodal capacitance	C_m	0.0714	pF	[50]
Nodal resistance	R_m	1953.49	M Ω	[50]
Na reversal pot.	E_{Na}	66	mV	[49]
K reversal pot.	E_K	-88	mV	[49]
HCNv Reversal pot.	E_h	-43	mV	[36]
Resting membrane pot.	V_{rest}	-78	mV	[49]
Na conductance	γ_{Na}	25.69	pS	[49]
Kv conductance	γ_{Kv}	50.0	pS	[23]
KLT conductance	γ_{KLT}	13.0	pS	text
HCN conductance	γ_h	13.0	pS	text
Max# Na channels	N_{Na}^{max}	1000		[49]
Max# Kv channels	N_{Kv}^{max}	166		text
Max# KLT channels	N_{KLT}^{max}	166		text
Max# HCN channels	N_h^{max}	100		text
KLT thermal coeff.	$Q_{10_{KLT}}$	3.0		text
HCN thermal coeff.	Q_{10_h}	3.3		text

The membrane equation of the model is given by the first-order differential equation

$$C_m \frac{dV_m}{dt} + I_{Na} + I_K + I_{KLT} + I_h + I_{lk} = I_{inj} \quad (1)$$

where V_m is the membrane potential, C_m is the membrane capacitance, and I_{inj} is the stimulus current.

A channel-number-tracking (CNT) algorithm [48] was utilized to represent the stochastic fast sodium [49] and delayed-rectifier potassium [23] channels. Independent gating particles were assumed to follow a Markov jumping process [23], [49]. The Markov jumping process approach and the CNT algorithm were extended to represent stochastic gating particles of HCN and KLT channels. The model ion channel kinetics were set for a mammalian body temperature of 37 °C. A complete list of equations is given in the Appendix.

B. Stimuli

For simulations of pulse train responses, the model behavior was simulated for a period of 200 ms without any current injection, to allow for fluctuations in the stochastic model away from the initial conditions, and was subsequently injected intracellularly by a continuous train of current pulses for 300 ms. Each pulse was a symmetric, charge-balanced, biphasic, depolarizing-phase-leading pulse with a duration of 50 μ s/phase and no interphase gap. Stimulus rates were chosen at rates similar to those used in CIs [12], [13].

For the refractory analysis, a pair of symmetric, charge-balanced, biphasic, depolarizing-phase-leading pulses were utilized. The pulses were 75 μ s/phase with an interphase gap of 75 μ s/phase. The amplitude of the first pulse was sufficiently large (50 pA) to always generate an action potential, and the second pulse was varied in amplitude to determine the firing efficiency (FE) versus level functions for the second pulse at a range of interpulse intervals (IPIs).

C. Data Analysis

The responses of four versions of the model were compared. These versions are: 1) the standard (stochastic) HH model; 2) the HH model with I_h alone added; 3) the HH model with I_{KLT} alone added; and 4) the HH model with both I_h and I_{KLT} added. The membrane potential was calculated by integrating (1) using Euler's method with a time step of 1 μ s.

The stimulus current for a stochastic ion channel is represented in terms of FE, which is an estimate of the probability of a nerve fiber to create an action potential in response to a certain current stimulus input level [16]. The relation governing the spiking probability and the stimulus level is well fit by an integrated-Gaussian function

$$FE = \frac{1}{2} \left(\operatorname{erf} \left(\frac{I - \theta}{\sqrt{2}\sigma} \right) + 1 \right) \quad (2)$$

where θ is the mean threshold current (i.e., corresponding to a FE of 50%) and σ is the standard deviation in threshold fluctuations [16]. The FE versus level function for each model was calculated for a single-pulse stimulus by running 1000 Monte-Carlo simulations.

For the pulse-pair paradigm to test the refractory behavior, the recovery of the threshold current (θ) for the second pulse as a function of IPI was fit by

$$\theta = \frac{\theta_{SP} (A_1 + A_2)}{A_1(1 - e^{-(IPI - t_{abs})/\tau_1}) + A_2(1 - e^{-(IPI - t_{abs})/\tau_2})} \quad (3)$$

where θ_{SP} is the single-pulse (or unmasked) threshold current, t_{abs} is the absolute refractory period, and τ_1 , τ_2 , A_1 , and A_2 are, respectively, the time constants and strengths of two relative refractory period components. This function is a generalization of [4, (2)], which only had a single time-constant for the relative refractory period, i.e., was equivalent to (3) above with $A_2 = 0$. We found that this extended equation with two components to the relative refractory period provided better fits to some of the simulation results.

The peri-stimulus time histogram (PSTH) is defined as the number of spikes created within a certain time frame from stimulus onset. PSTHs were computed from 100 repetitions of Monte-Carlo simulation, where two categories of time bin widths were defined [12]: 1) a "narrow bin" width of 1 ms; and 2) a group of eight nonoverlapping "wide bin" windows. These windows were 0–4, 4–12, 12–24, 24–36, 36–48, 48–100, 100–200, and 200–300 ms after pulse-train onset.

To analyze response rate adaptation [12], the response rate as a function of stimulus current was investigated with a stimulus at a pulse rate of 2000 pulse/s. Three different response epochs were specified. These epochs are denoted as in [12]: "onset" (0–1 ms); "rapid" (0–12 ms); and "short-term" or "steady-state" (200–300 ms). For more quantitative analysis on response rate adaptation, two variables were computed [12]. These are, spike rate decrement (SRD), which was calculated by subtracting the spike rate in the steady-state epoch (200–300 ms) from that in the onset window (0–12 ms); and the normalized spike rate decrement (NSRD), which was the SRD divided by the onset response. Two regions of adaptation were defined [12]:

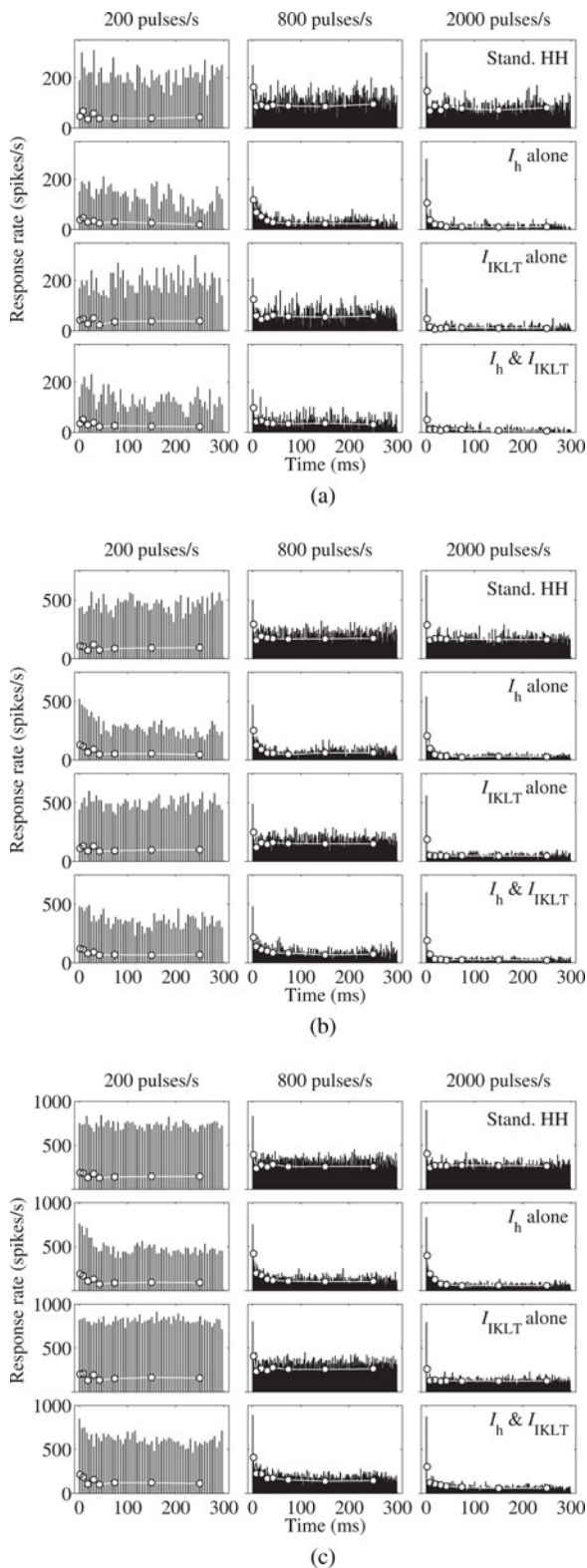


Fig. 2. PSTH from the response of the four model versions (rows) at stimulus pulse rates of 200, 800, and 2000 pulse/s (columns). (a), (b), and (c) represent stimulus levels at 0.2, 0.5, and 0.8 firing probability to the first pulse. Thin vertical bars represent histograms based on 1-ms bins, while open symbols represent wider bins. Histograms are obtained from 100 simulation trials. (a) First-pulse FE = 20%. (b) First-pulse FE = 50%. (c) First-pulse FE = 80%.

“strong” (in gray) and “weak.” The strong adaptation areas in each panel were bounded by arbitrarily defined slope values between 0.75 and 1.0. It is worth noting that these strong adaptation boundaries were somewhat different from those defined in [12], whereas they chose an area between 0.9 and 1.0.

III. RESULTS

A. Poststimulus Time Histograms

The PSTH results are shown in Fig. 2. The narrow bins are represented by vertical bars and the wide bins with unfilled circles. The wide bins showed more accurately the trend of spike rate over a long period of time than the narrow bins [12]. The four model versions were stimulated at 200, 800, and 2000 pulse/s (left, middle, and right columns, respectively) and stimulus level at 0.2, 0.5, and 0.8 firing probabilities (Fig. 2(a)–(c), respectively) to the first pulse. Comparisons are made based on equal first-pulse FEs because the model variants have different threshold currents and dynamic ranges [46]. For these simulations, the threshold currents (i.e., at FE = 0.5) for the four models (Standard HH, I_h alone added, I_{KLT} alone added, and with both I_h and I_{KLT} added) are 54.29, 59.68, 57.36, and 62.70 pA, respectively. For an FE of 0.2, the respective stimulation levels are 52.98, 57.10, 54.98, and 60.00 pA, while for an FE 0.8 they are 55.59, 62.26, 59.75, and 65.40 pA.

Across all stimulus rates for the standard HH case, a flat wide bins curve is observed indicating no adaptation, except at the 2000 pulse/s (see Fig. 2(a), first row, right panel), where the spike rate drops slightly. This could be attributed to the low discharge probability and the refractory effect rather than adaptation, as at higher stimulus levels the model maintains a constant spike rate (Figs. 2(b) and (c), first row, right panel). The model shows strong adaptation when the I_h is included [second row, Figs. 2(a)–(c)] at higher stimulus rates, as indicated by the exponential decay of the wide-bin curve. The drop in response rate dominates even at higher discharge probabilities. Adding I_{KLT} only (third rows), causes the spike rate to drop at the first few milliseconds (not as much as the I_h case) and remains at the reduced level throughout the stimulation period. The inclusion of both I_h and I_{KLT} simultaneously (fourth rows) produces a combined effect that exhibits the response of each channel when added solely.

B. Response Rate Adaptation Analysis

The response rate was plotted as a function of stimulus current [12] for the four model versions, as shown in Fig. 3. The onset response was influenced by refractory and discharge probability effects, preventing the spike rate to entrain to the stimulus rate. I_{KLT} with (■) or without (◆) I_h showed lower response rates at the onset and rapid epochs than the standard HH model (●) and when I_h is added alone (▲), when comparing response rates at the same FE to the first pulse. This could be an indication of rapid adaptation. I_h alone or with I_{KLT} had shallower slopes than the standard HH model and I_{KLT} alone for the steady-state epoch. The standard HH model showed no

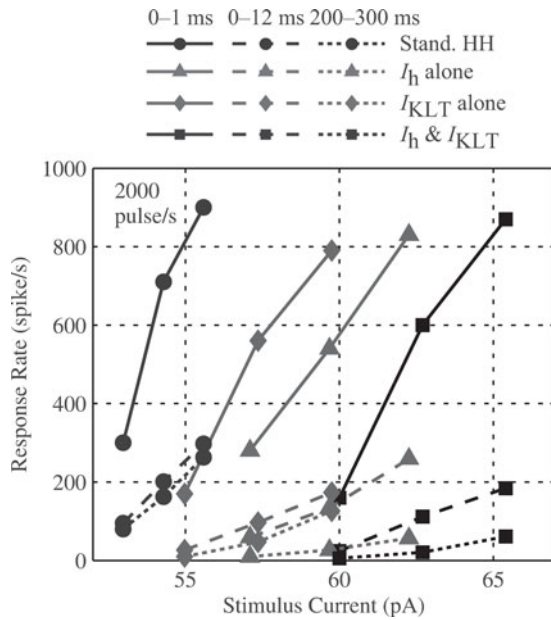


Fig. 3. Response rate as a function of stimulus level at three different epochs. Analysis windows are 0–1 ms (—), 0–12 ms (---), and 200–300 ms (···), after stimulus onset. Stimulus rate is 2000 pulse/s. Different model versions are represented by filled symbols.

difference in response rate between the rapid and short-term epochs. These results suggested that I_h was responsible for short-term adaptation. Results from Fig. 3 were comparable to [12, Fig. 4, p. 361], where the “rapid” and “steady-state” epochs responses were apart, with the “steady-state” response being the lowest. Note that the stimulus pulse rate in Zhang *et al.* figure was 5000 pulse/s.

Fig. 4 shows the SRDs (spike rate during 0–12 ms minus spike rate during 200–300 ms) in the left column and NSRDs in the right column as a function of onset response rate (spike rate during 0–12 ms), for three stimulus pulse rates: 200, 800, and 2000 pulse/s (Fig. 4(a) and (b); Fig. 4(c) and (d); and Fig. 4(e) and (f), respectively). In all pulse rate cases, the standard HH model (\bullet) showed almost zero rate decrement, which could be interpreted as weak or no adaptation. Adding I_h only (\blacktriangle) on the other hand showed strong adaptation, which became stronger at higher pulse rates. With inclusion of both I_h and I_{KLT} (\blacksquare), the response tended toward stronger adaptation, however, slightly less than when I_h was added alone. I_{KLT} alone (\blacklozenge) exhibited stronger adaptation than the standard HH model, yet weaker than the other two versions. These results were consistent with [12, Fig. 5, p. 363], where SRDs became equal to onset response rate, when the stimulus pulse rate was increased. Looking at panels (b), (d), and (f), the normalized rate decrements became smaller at higher onset spike rates that were greater than 200 spike/s, consistent with [12] who suggested that this effect might result from greater stimulus levels that could partially overcome adaptation.

To gain more insight into how the I_h channel produces the slow drop in excitability, the model with I_h alone added was subjected to a set of different stimulation and response scenarios,

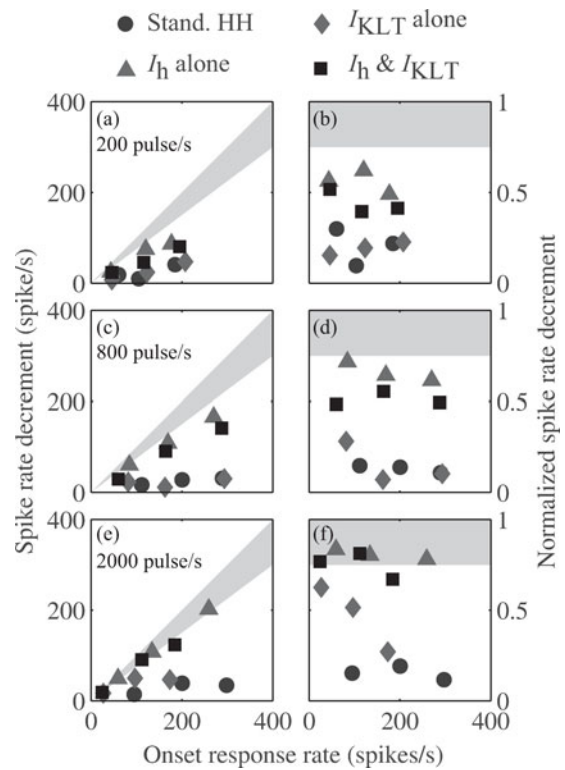


Fig. 4. SRD (left column) and NSRD (right column) as a function of onset response rate, for pulse rates of 200, 800, and 2000 pulse/s (a & b; c & d; and e & f, respectively). The gray region indicates “strong adaptation” and is arbitrarily chosen to be ≥ 0.75 of the normalized rate decrement. The model versions are indicated by the figure legend.

as shown in Fig. 5. In all cases, the model was stimulated by pulse trains at 2000 pulse/s with pulse width of 100 μ s/phase and no interphase gap for a duration of 20 ms (\equiv 40 pulses).

The relatively short simulation duration (compared to the 300-ms PSTH simulations) is because short-term adaptation in this model appears at about 15 ms after stimulus onset. Fig. 5(a) shows the average relative membrane potential² for the last 100 μ s of the interpulse gap, i.e., before the subsequent pulse. Each point in each of the curves corresponds to the mean of the averaged voltage for 50 Monte-Carlo simulation for that particular stimulation-response scenario. Fig. 5(b) shows the average fraction of open I_h channel gating particles (\hat{r}) at the corresponding times. Five specific stimulation-response conditions are defined: “zero current” (\circ), “no spike” (\triangle), “first pulse” (\diamond), “middle pulse” (\square), and “suprathreshold” (*).

In the “zero current” condition (\circ), no stimulating current was applied. It can be observed in Fig. 5 that for this scenario there is minimal fluctuation in the average relative membrane potential and the average fraction of open I_h channel gating particles over the duration of the pulse train for the 50 Monte-Carlo simulations. In the “no spike” case (\triangle), the stimulating current amplitude for the pulse train was set to give a first-pulse firing probability of 0.2, but only Monte-Carlo simulation trials

²The relative membrane potential $V(t)$ is the difference between the membrane potential $V_m(t)$ and resting potential V_{rest} , i.e., $V(t) = V_m(t) - V_{rest}$.

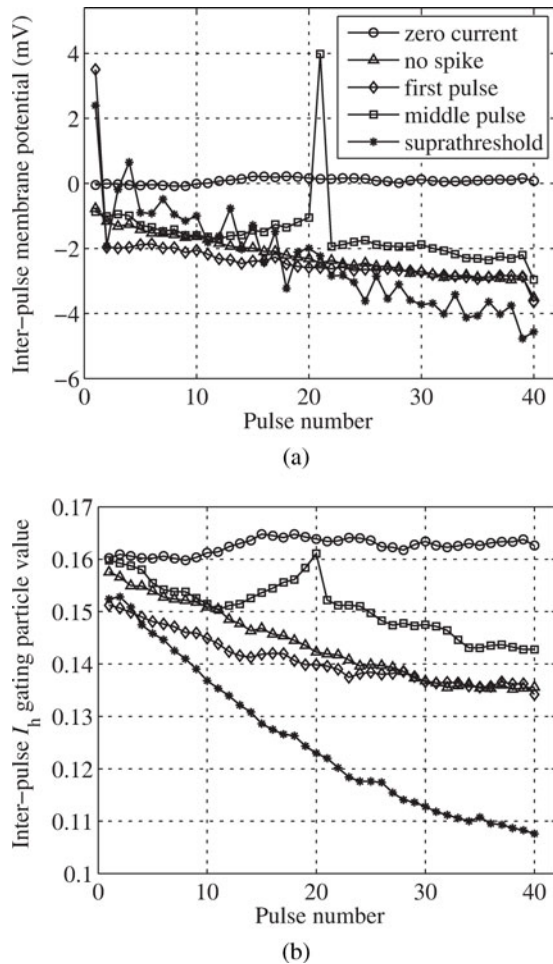


Fig. 5. Comparison between five stimulation-response scenarios (listed in the figure legend and described in the text) for the model with I_h added alone. (a) Mean relative membrane potential in the interpulse gaps (averaged over 50 Monte-Carlo stimulations) as a function of pulse number. (b) Mean I_h gating particle values in the interpulse gaps (averaged over 50 Monte-Carlo stimulations) as a function of pulse number.

in which no spike was generated during the pulse train were selected for computation of the mean interpulse membrane potential and gating particle value for the curves in Fig. 5. The repetitive subthreshold responses in this situation cause a progressive drop in the fraction of open I_h channel gating particles (see Fig. 5b), which in turn leads to a progressive drop in the membrane potential between each stimulating pulse (see Fig. 5a). Thus, the successive subthreshold responses move the membrane potential further away from the threshold for action potential generation, reducing excitability gradually.

In the “first pulse” case (\diamond), only Monte-Carlo trials were selected in which the first current pulse elicited an action potential and there were no subsequent action potentials in response to the rest of the pulse train. Again, the first pulse FE was 0.2. In this situation, the action potential in response to the first pulse causes a bigger initial drop in the fraction of open I_h channel gating particles (see Fig. 5b) and in the interpulse membrane potential (see Fig. 5a) than did the subthreshold first pulse for the “no spike” case, but by the end of the 40 stimulating

pulses the average fraction of open r particles and the average interpulse membrane potential have both converged for the two cases. In the “middle pulse” case (\circ), once again the first pulse FE was 0.2, but trials were selected in which one action potential was generated in response to the 20th pulse in the train and no other action potentials were generated for that pulse train. In such trials, it can be observed that the response to the first ten pulses or so is very similar on average to the “no spike” trials (see Fig. 5b). However, in trials where a spike occurs in the middle of the pulse train, the random fluctuations of the I_h channel gating particles happen to return the fraction of open I_h channels (see Fig. 5b) and subsequently the interpulse membrane potential (see Fig. 5a) back toward their resting values, such that the neural excitability is closer to its resting state. This result illustrates the importance of utilizing a stochastic model when studying “subthreshold” membrane phenomena.

For the “suprathreshold” condition ($*$), a stimulating current level was chosen to give a 0.999 firing probability to the first pulse, such that the vast majority of the pulses would elicit action potentials if not for the temporal interactions from the pulse train. In this situation, the fraction of open I_h channel gating particles drops at a greater rate than is observed for the “no spike” or “first pulse” conditions (see Fig. 5b), indicating that the larger subthreshold responses from the larger stimulating current and the larger depolarizations from the occasional spiking cause a more rapid drop in excitability than do the smaller subthreshold responses from the “no spike” or “first pulse” conditions. The interpulse membrane potential is initially high for the “suprathreshold” case (see Fig. 5a) because of the more frequent spiking at the start of the pulse train, but the interpulse membrane potential drops substantially as the I_h channels close up later in the pulse train and the spike rate drops dramatically. Some alternation in the interpulse membrane potential is also observed at the start of the pulse train because refractoriness makes the neural model more likely to spike in response to pulses 1 and 3 than to pulses 2 and 4, and the interpulse membrane potential is high during an action potential (also seen where a spike is generated in the “first pulse” and “middle pulse” conditions).

C. Refractoriness

Fig. 6 shows the models’ refractory behavior using a pulse-pair paradigm based on [4]. The symbols in Fig. 6 show the recovery of the threshold current, determined by fits using (2) and normalized by the single-pulse threshold current, as a function of the IPI. The symbols used to plot the results for the different model versions are indicated by the legend. The solid lines are fits to these curves using (3), and the parameters for these fits are given in Table II.

The addition of the I_h channel (\blacktriangle) to the HH model (\bullet) increases the initial relative refractory period without changing the absolute refractory period or the slower component of the relative refractory recovery. In contrast, adding I_{KLT} (\blacklozenge) to the HH model increases the absolute refractory period and both the fast and slow components of relative refractory period. This increased period of refractoriness occurs during a period of

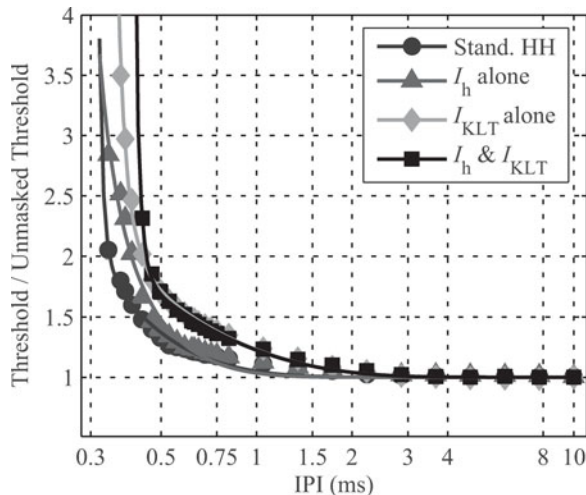


Fig. 6. Refractory recovery functions of threshold currents for the four different models.

TABLE II
REFRACTORY FUNCTION FITS FOR THE FOUR MODELS

Value	Stand. HH	I_h alone	I_{KLT} alone	I_h and I_{KLT}
A_1	1.71	0.92	1.36	1.62
A_2	1.89	2.91	1.49	1.40
t_{abs} (ms)	0.31	0.31	0.34	0.40
τ_1 (μ s)	13.4	0.87	41.6	22.1
τ_2 (ms)	0.29	0.22	0.64	0.64

TABLE III
SENSITIVITY ANALYSIS FOR THE NUMBER OF ION CHANNELS

Value	Effect of N_h^{max} $\times 0 : \times 1/2 : \times 1 : \times 2$	Effect of N_{KLT}^{max} $\times 0 : \times 1/2 : \times 1 : \times 2$
MNSRD200	0.20 : 0.46 : 0.56 : 0.50	0.20 : 0.19 : 0.19 : 0.21
MNSRD800	0.13 : 0.63 : 0.66 : 0.68	0.13 : 0.03 : 0.15 : 0.13
MNSRD2000	0.15 : 0.75 : 0.81 : 0.83	0.15 : 0.37 : 0.47 : 0.56
A_1	1.71 : 0.37 : 0.92 : 2.46	1.71 : 0.75 : 1.36 : 1.73
A_2	1.89 : 1.07 : 2.91 : 3.00	1.89 : 1.61 : 1.49 : 2.03
t_{abs} (ms)	0.31 : 0.31 : 0.31 : 0.39	0.31 : 0.31 : 0.34 : 0.40
τ_1 (μ s)	13.4 : 0.21 : 0.87 : 12.0	13.4 : 28.1 : 42.0 : 18.1
τ_2 (ms)	0.29 : 0.21 : 0.22 : 0.24	0.29 : 0.35 : 0.64 : 0.72

MNSRD200, MNSRD500, and MNSRD2000 refer to the MNSRD at 200, 800 and 2,000 pps, respectively.

afterhyperpolarization that does not occur for the standard HH model. Including both channel types in the model (■) produces a synergistic increase of the absolute refractory period, while the slower component of the relative refractory period remains dominated by the I_{KLT} channel.

Care must be taken in comparing time constants for the relative refractory period components in Tables II and III because the effect of the component is also determined by the relative magnitude of that component.

D. Sensitivity Analysis

The results of an analysis of the sensitivity of the simulation results to the number of HCN and KLT channels are given in Table III. Simulations were performed with zero, half, and double the default number of HCN and KLT channels (given in Table I). In order to capture the effect of channel number on adaptation in the PSTH in a single value, the mean normalized spike rate decrement (MNSRD) was calculated across the three different first-pulse firing efficiencies ($FE = 20\%$, 50% , and 80%). The effect of channel number on the refractory function fits was also explored. This analysis shows a general trend of an increased strength of adaptation and refractoriness with larger numbers of HCN and KLT channels. However, even with half the default number of channels (indicated by $\times 1/2$ in Table III), the versions of the model with the additional channels show a marked qualitative difference to the standard HH model (indicated by $\times 0$ in Table III). This suggests that it is not necessary for a node of Ranvier to have very large numbers of KLT or HCN channels to produce a functional change in the temporal interactions exhibited at that node.

IV. DISCUSSION

The simulation results shown in this paper demonstrate that HCN and KLT channels could have substantial effects on the temporal response properties of ANFs to electrical pulse trains from CIs. The I_h current carried by the HCN channels appears to produce slow adaptation to an ongoing pulse train, while the I_{KLT} generated by the KLT channels has a faster effect (see Figs. 2–4). The strength of the adaptation, as quantified in the normalized rate decrements shown in Fig. 4, appears to be slightly stronger for I_h than I_{KLT} . However, because of the faster rate of adaptation and longer refractoriness (see Fig. 6) caused by I_{KLT} , the rate calculated in this metric may already be reduced within the onset response window, leading to an underestimation of the strength of adaptation produced by I_{KLT} . The analysis shown in Fig. 5 indicates that the gradual drop in excitability of a model with I_h for a high-rate pulse train is due not only to spike-rate adaptation but also to subthreshold responses (i.e., pulses that do not elicit an action potential). Such behavior has been referred to in the CI literature as desensitization [8] or subthreshold masking [10], but the historical terminology is accommodation [51], [52]. All of the simulations reported in this paper were conducted with a stochastic model. The effect of HCN and KLT channels on the refractory recovery are fundamentally the same if simulated using equivalent deterministic models. Dynamic instability in a deterministic neural model has been shown to produce irregular firing for very high rates of stimulation [53], but the equivalent deterministic models of those used in the present study do not exhibit adaptation or accommodation that is consistent with the physiological data across the appropriate pulse rates and current levels.

An alternative mechanism for adaptation and accommodation based on extracellular potassium accumulation has been proposed by Woo *et al.* [10], [26]–[28]. Accommodation could only be generated in their model if it included a KLT channel [10]. However, they could not determine a set of ion channel

densities that could simultaneously explain the physiological data for rate adaptation, adaptation recovery, and refractory periods [10]. Based on the results of this present study, inclusion of an I_h model might be required to properly explain all the contributing factors to refractoriness, adaptation, and accommodation. In addition, Miller *et al.* utilized an I_{KLT} model incorporating only a single activation particle and no inactivation [10] that was based on channels in nonauditory neurons, following [25]. However, the I_{KLT} properties of SGNs [32], [33] appear to be closer to those of VCN cells [41], [44], [45] and MSO neurons [39], motivating our use of the channel model from [36] with fourth-order activation kinetics and partial inactivation.

Inclusion of I_h and I_{KLT} was found to systematically change refractory properties of model ANFs (see Fig. 6). Variation in HCN and KLT channel densities at different nodes of Ranvier may, therefore, explain the variability observed in refractory properties of cat ANFs [3], [4]. However, the model developed in this study is unable to predict the extension of relative refractoriness out to at least 4 ms in a subpopulation of ANFs that is observed in the cat and human physiological data [3], [4], [6], [7]. Our sensitivity analysis only considered the effects of the number of channels. Other parameters such as nodal geometry, single-channel conductances, and activation/inactivation dynamics may also influence the refractory and adaptation properties. In particular, there is a fair degree of heterogeneity in the activation and inactivation characteristics of HCN [30] and KLT [44], [45] channels. It is also possible that yet further ion channels with slow dynamics, beyond HCN and KLT, are contributing to refractory and adaptation properties at these longer time periods. A multiplicity of contributing ion channels with a large range of time constants can give rise to “power-law adaptation” [54], which has been found to be important in modeling the response of ANFs to acoustic stimulation [55], [56].

There may also be species differences in the ion channels expressed in ANFs, such as the persistent sodium channel that has been incorporated into a model of human ANFs [57]–[59]. It is not yet known whether a persistent sodium channel exists in the ANFs of other species such as cat. In this paper, we have used a single-node model in order to separate out the effects of the HCN and KLT channels from other factors that could influence the temporal response properties, such as the neural morphology and the electrode–neuron geometry [23], [28]. The neural morphology is known to vary across species as well, motivating the development of species-specific compartmental models of entire ANFs, where possible [20], [57]–[61]. In all cases, the particular locations of different voltage-gate ion channels, including HCN and KLT, along the ANFs should be taken into consideration [34], [62].

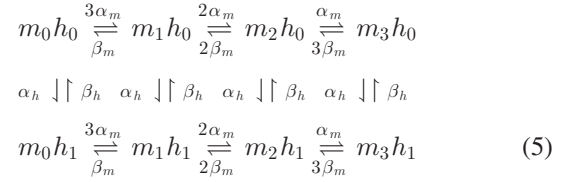
APPENDIX

The four voltage-gated ion channel currents are modeled using the following equations:

Nav Channel:

$$I_{Na}(t) = \gamma_{Na} N_{m_3 h_1}(t) [V_m(t) - E_{Na}] \quad (4)$$

where $N_{m_3 h_1}$ is the number of Nav channels in the conducting state, determined by a Markov process with the kinetic scheme



and the transition rates (in units of $m \cdot s^{-1}$) depend on the relative membrane potential V according to

$$\alpha_m(V) = \frac{1.872(V - 25.41)}{1 - \exp((25.41 - V)/6.06)} \quad (6)$$

$$\beta_m(V) = \frac{3.973(21.001 - V)}{1 - \exp((V - 21.001)/9.41)} \quad (7)$$

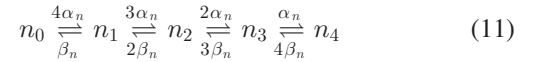
$$\alpha_h(V) = \frac{-0.549(27.74 + V)}{1 - \exp((V + 27.74)/9.06)} \quad (8)$$

$$\beta_h(V) = \frac{22.57}{1 + \exp((56.0 - V)/12.5)}. \quad (9)$$

Kv Channel:

$$I_K(t) = \gamma_K N_{n_4}(t) [V_m(t) - E_K] \quad (10)$$

where N_{n_4} is the number of Kv channels in the conducting state, determined by the kinetic scheme



and the transition rates are

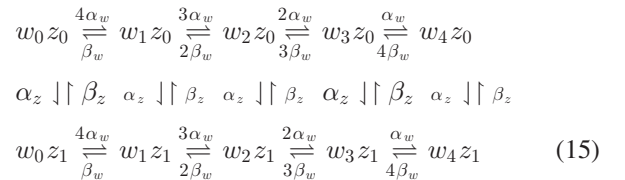
$$\alpha_n(V) = \frac{0.129(V - 35)}{1 - \exp((35 - V)/10)} \quad (12)$$

$$\beta_n(V) = \frac{0.3236(35 - V)}{1 - \exp((V - 35)/10)}. \quad (13)$$

KLT Channel:

$$I_{KLT}(t) = \gamma_{KLT} N_{w_4 z_1}(t) [V_m(t) - E_K] \quad (14)$$

where $N_{w_4 z_1}$ is the number of KLT channels in the conducting state, determined by the kinetic scheme



and the transition rates are

$$\alpha_w(V) = w_\infty(V) / \tau_w(V) \quad (16)$$

$$\beta_w(V) = (1 - w_\infty(V)) / \tau_w(V) \quad (17)$$

where

$$w_\infty(V) = \frac{1}{(\exp(13/5 - V/6) + 1)^{1/4}} \quad (18)$$

$$\tau_w(V) = 0.2887 + \frac{17.53 \exp\left(\frac{V}{45}\right)}{\left(3 \exp\left(\frac{17V}{90}\right) + 15.791\right)} \quad (19)$$

and

$$\alpha_z(V) = z_\infty(V) / \tau_z(V) \quad (20)$$

$$\beta_z(V) = (1 - z_\infty(V)) / \tau_z(V) \quad (21)$$

where

$$z_\infty(V) = \frac{1}{2 \left(\exp(V/10 + 0.74) + 1 \right)} + 0.5 \quad (22)$$

$$\tau_z(V) = 9.6225 + \frac{2073.6 \exp\left(\frac{V}{8}\right)}{9 \left(\exp\left(\frac{7V}{40}\right) + 1.8776 \right)}. \quad (23)$$

HCN Channel:

$$I_h(t) = \gamma_h N_{r_1}(t) [V_m(t) - E_h] \quad (24)$$

where N_{r_1} is the number of HCN channels in the conducting state, determined by the kinetic scheme

$$r_0 \xrightleftharpoons[\beta_r]{\alpha_r} r_1 \quad (25)$$

and the transition rates are

$$\alpha_r(V) = r_\infty(V) / \tau_r(V) \quad (26)$$

$$\beta_r(V) = (1 - r_\infty(V)) / \tau_r(V) \quad (27)$$

where

$$r_\infty(V) = \frac{1}{\left(\exp(V/7 + 62/35) + 1 \right)} \quad (28)$$

$$\tau_r(V) = \frac{50000}{711 \exp\left(\frac{V}{12} - \frac{3}{10}\right) + 51 \exp\left(\frac{9}{35} - \frac{V}{14}\right)} + \frac{25}{6}. \quad (29)$$

Modifications From VCN Cell and Squid Giant Axon Channel Models:

Note that the original HCN and KLT channel transition rate equations for τ_w , τ_z , and τ_r from [36] were divided by the thermal coefficient constants [15] k_w , k_z , and k_r , respectively, to produce (19), (23), and (29). The thermal coefficient constant is

$$k_x = Q10_x^{(T-T_0)/10.0} \quad (30)$$

where x denotes w , z or r , $Q10$ is the gain increase for every 10 °C (given in Table I), T_0 is the original temperature, and T is the desired temperature.

In addition, the activation/inactivation curves were shifted to account for the difference in resting membrane potential of the AN node of Ranvier model in this paper and the VCN cell model in [36].

The equations for the Nav and Kv channels were already appropriate for the desired AN node of Ranvier temperature and resting potential [23], [49]. Note that the dynamics of these channels in [23], [49] were modified somewhat from the original HH model of the squid giant axon [14] to give a more realistic AP waveform at 37 °C.

ACKNOWLEDGMENT

The authors would like to thank Dr. R. Davis and Dr. P. Manis for advice on model parameters values, Dr. M. White and Dr. L. Cohen for many helpful discussions on the physiological data, and Mr. J. Boulet and two anonymous reviewers for helpful comments on previous versions of the manuscript. Part of this study was conducted while I. Bruce was a Visiting Scholar at the Bionic Ear Institute, Melbourne, Vic., Australia.

REFERENCES

- [1] B. S. Wilson, C. C. Finley, J. Farmer, Jr., D. T. Lawson, B. A. Weber, R. D. Wolford, P. D. Kenan, M. W. White, M. M. Merzenich, and R. A. Schindler, "Comparative studies of speech processing strategies for cochlear implants,," *Laryngoscope*, vol. 98, no. 10, pp. 1069–1077, Oct. 1988.
- [2] K. Arora, P. Dawson, R. Dowell, and A. Vandali, "Electrical stimulation rate effects on speech perception in cochlear implants,," *Int. J. Audiol.*, vol. 48, no. 8, pp. 561–567, Aug. 2009.
- [3] L. A. Cartee, C. van den Honert, C. C. Finley, and R. L. Miller, "Evaluation of a model of the cochlear neural membrane. I: Physiological measurement of membrane characteristics in response to intrameatal electrical stimulation,," *Hear. Res.*, vol. 146, no. 1–2, pp. 143–152, Aug. 2000.
- [4] C. A. Miller, P. J. Abbas, and B. K. Robinson, "Response properties of the refractory auditory nerve fiber,," *J. Assoc. Res. Otolaryngol.*, vol. 2, no. 3, pp. 216–232, Sep. 2001.
- [5] L. A. Cartee, C. A. Miller, and C. van den Honert, "Spiral ganglion cell site of excitation I: Comparison of scala tympani and intrameatal electrode responses,," *Hear. Res.*, vol. 215, no. 1–2, pp. 10–21, May 2006.
- [6] L. T. Cohen, "Practical model description of peripheral neural excitation in cochlear implant recipients: 5. Refractory recovery and facilitation,," *Hear. Res.*, vol. 248, no. 1–2, pp. 1–14, Feb. 2009.
- [7] A. Botros and C. Psarros, "Neural response telemetry reconsidered: II. The influence of neural population on the ECAP recovery function and refractoriness,," *Ear Hear.*, vol. 31, no. 3, pp. 380–391, Jun. 2010.
- [8] S. Dynes, "Discharge characteristics of auditory nerve fibers for pulsatile electrical stimuli,," Ph.D. dissertation, Massachusetts Inst. Technol., Cambridge, MA, USA, Feb. 1996.
- [9] L. F. Heffer, D. J. Sly, J. B. Fallon, M. W. White, R. K. Shepherd, and S. J. O'Leary, "Examining the auditory nerve fiber response to high rate cochlear implant stimulation: Chronic sensorineural hearing loss and facilitation,," *J. Neurophysiol.*, vol. 104, no. 6, pp. 3124–3135, Dec. 2010.
- [10] C. A. Miller, J. Woo, P. J. Abbas, N. Hu, and B. K. Robinson, "Neural masking by sub-threshold electric stimuli: Animal and computer model results,," *J. Assoc. Res. Otolaryngol.*, vol. 12, no. 2, pp. 219–232, Apr. 2011.
- [11] D. J. Sly, L. F. Heffer, M. W. White, R. K. Shepherd, M. G. J. Birch, R. L. Minter, N. E. Nelson, A. K. Wise, and S. J. O'Leary, "Deafness alters auditory nerve fibre responses to cochlear implant stimulation,," *Eur. J. Neurosci.*, vol. 26, no. 2, pp. 510–522, Jul. 2007.
- [12] F. Zhang, C. A. Miller, B. K. Robinson, P. J. Abbas, and N. Hu, "Changes across time in spike rate and spike amplitude of auditory nerve fibers stimulated by electric pulse trains,," *J. Assoc. Res. Otolaryngol.*, vol. 8, no. 3, pp. 356–372, Sep. 2007.
- [13] C. A. Miller, N. Hu, F. Zhang, B. K. Robinson, and P. J. Abbas, "Changes across time in the temporal responses of auditory nerve fibers stimulated by electric pulse trains,," *J. Assoc. Res. Otolaryngol.*, vol. 9, no. 1, pp. 122–137, Mar. 2008.
- [14] A. Hodgkin and A. Huxley, "A quantitative description of membrane current and its application to conduction and excitation in nerve,," *J. Physiol.*, vol. 117, pp. 500–544, 1952.
- [15] L. A. Cartee, "Evaluation of a model of the cochlear neural membrane. II: Comparison of model and physiological measures of membrane properties measured in response to intrameatal electrical stimulation,," *Hear. Res.*, vol. 146, no. 1–2, pp. 153–166, Aug. 2000.
- [16] A. A. Verveen and H. E. Derksen, "Fluctuation phenomena in nerve membrane,," *Proc. IEEE*, vol. 56, no. 6, pp. 906–916, Jun. 1968.
- [17] A. A. Verveen, "Axon diameter and fluctuation in excitability,," *Acta Morph. Neerl.-Scand.*, vol. 5, pp. 79–85, 1962.
- [18] I. C. Bruce, M. W. White, L. S. Irlicht, S. J. O'Leary, S. Dynes, E. Javel, and G. M. Clark, "A stochastic model of the electrically stimulated auditory

- nerve: Single-pulse response,” *IEEE Trans. Biomed. Eng.*, vol. 46, no. 6, pp. 617–629, Jun. 1999.
- [19] J. T. Rubinstein, “Threshold fluctuations in an N sodium channel model of the node of Ranvier,” *Biophys. J.*, vol. 68, pp. 779–785, Mar. 1995.
- [20] F. Rattay, P. Lutter, and H. Felix, “A model of the electrically excited human cochlear neuron. I. Contribution of neural substructures to the generation and propagation of spikes,” *Hear. Res.*, vol. 153, no. 1–2, pp. 43–63, Mar. 2001.
- [21] F. Rattay, R. N. Leao, and H. Felix, “A model of the electrically excited human cochlear neuron. II. Influence of the three-dimensional cochlear structure on neural excitability,” *Hear. Res.*, vol. 153, no. 1–2, pp. 64–79, Mar. 2001.
- [22] A. J. Matsuoka, J. T. Rubinstein, P. J. Abbas, and C. A. Miller, “The effects of interpulse interval on stochastic properties of electrical stimulation: Models and measurements,” *IEEE Trans. Biomed. Eng.*, vol. 48, no. 4, pp. 416–424, Apr. 2001.
- [23] H. Mino, J. T. Rubinstein, C. A. Miller, and P. J. Abbas, “Effects of electrode-to-fiber distance on temporal neural response with electrical stimulation,” *IEEE Trans. Biomed. Eng.*, vol. 51, no. 1, pp. 13–20, Jan. 2004.
- [24] H. Mino and J. T. Rubinstein, “Effects of neural refractoriness on spatio-temporal variability in spike initiations with electrical stimulation,” *IEEE Trans. Neural Syst. Rehabil. Eng.*, vol. 14, no. 3, pp. 273–280, Sep. 2006.
- [25] N. S. Imennov and J. T. Rubinstein, “Stochastic population model for electrical stimulation of the auditory nerve,” *IEEE Trans. Biomed. Eng.*, vol. 56, no. 10, pp. 2493–2501, Oct. 2009.
- [26] J. Woo, C. A. Miller, and P. J. Abbas, “Simulation of the electrically stimulated cochlear neuron: Modeling adaptation to trains of electric pulses,” *IEEE Trans. Biomed. Eng.*, vol. 56, no. 5, pp. 1348–1359, May 2009.
- [27] J. Woo, C. A. Miller, and P. J. Abbas, “Biophysical model of an auditory nerve fiber with a novel adaptation component,” *IEEE Trans. Biomed. Eng.*, vol. 56, no. 9, pp. 2177–2180, Sep. 2009.
- [28] J. Woo, C. A. Miller, and P. J. Abbas, “The dependence of auditory nerve rate adaptation on electric stimulus parameters, electrode position, and fiber diameter: A computer model study,” *J. Assoc. Res. Otolaryngol.*, vol. 11, no. 2, pp. 283–296, Jun. 2010.
- [29] J. Santos-Sacchi, “Voltage-dependent ionic conductances of type I spiral ganglion cells from the guinea pig inner ear,” *J. Neurosci.*, vol. 13, no. 8, pp. 3599–3611, Aug. 1993.
- [30] Z. L. Mo and R. L. Davis, “Heterogeneous voltage dependence of inward rectifier currents in spiral ganglion neurons,” *J. Neurophysiol.*, vol. 78, no. 6, pp. 3019–27, Dec. 1997.
- [31] C. Chen, “Hyperpolarization-activated current (I_h) in primary auditory neurons,” *Hear. Res.*, vol. 110, no. 1–2, pp. 179–90, Aug. 1997.
- [32] Z. L. Mo, C. L. Adamson, and R. L. Davis, “Dendrotoxin-sensitive K currents contribute to accommodation in murine spiral ganglion neurons,” *J. Physiol.*, vol. 542, no. 3, pp. 763–778, 2002.
- [33] C. L. Adamson, M. A. Reid, Z.-L. Mo, J. Bowne-English, and R. L. Davis, “Firing features and potassium channel content of murine spiral ganglion neurons vary with cochlear location,” *J. Comp. Neurol.*, vol. 447, no. 4, pp. 331–350, Jun. 2002.
- [34] E. Yi, I. Roux, and E. Glowatzki, “Dendritic HCN channels shape excitatory postsynaptic potentials at the inner hair cell afferent synapse in the mammalian cochlea,” *J. Neurophysiol.*, vol. 103, no. 5, pp. 2532–2543, May. 2010.
- [35] N. L. Golding, M. J. Ferragamo, and D. Oertel, “Role of intrinsic conductances underlying responses to transients in octopus cells of the cochlear nucleus,” *J. Neurosci.*, vol. 19, no. 8, pp. 2897–2905, Apr. 15, 1999.
- [36] J. S. Rothman and P. B. Manis, “The roles potassium currents play in regulating the electrical activity of ventral cochlear nucleus neurons,” *J. Neurophysiol.*, vol. 89, no. 6, pp. 3097–3113, Jun. 2003.
- [37] A. R. A. Rodrigues and D. Oertel, “Hyperpolarization-activated currents regulate excitability in stellate cells of the mammalian ventral cochlear nucleus,” *J. Neurophysiol.*, vol. 95, no. 1, pp. 76–87, 2006.
- [38] R. Bal and D. Oertel, “Hyperpolarization-activated, mixed-cation current (I_h) in octopus cells of the mammalian cochlear nucleus,” *J. Neurophysiol.*, vol. 84, no. 2, pp. 806–817, Aug. 2000.
- [39] S. Khurana, M. W. H. Remme, J. Rinzel, and N. L. Golding, “Dynamic interaction of I_h and I_{K-LVA} during trains of synaptic potentials in principal neurons of the medial superior olive,” *J. Neurosci.*, vol. 31, no. 24, pp. 8936–8947, Jun. 2011.
- [40] X. W. Fu, B. L. Brezden, and S. H. Wu, “Hyperpolarization-activated inward current in neurons of the rat’s dorsal nucleus of the lateral lemniscus in vitro,” *J. Neurophysiol.*, vol. 78, no. 5, pp. 2235–2245, 1997.
- [41] R. Bal and D. Oertel, “Potassium currents in octopus cells of the mammalian cochlear nucleus,” *J. Neurophysiol.*, vol. 86, no. 5, pp. 2299–2311, Nov. 2001.
- [42] D. S. Bortone, K. Mitchell, and P. B. Manis, “Developmental time course of potassium channel expression in the rat cochlear nucleus,” *Hear. Res.*, vol. 211, no. 1–2, pp. 114–125, Jan. 2006.
- [43] Z. L. Mo and R. L. Davis, “Endogenous firing patterns of murine spiral ganglion neurons,” *J. Neurophysiol.*, vol. 77, no. 3, pp. 1294–1305, 1997.
- [44] J. S. Rothman and P. B. Manis, “Differential expression of three distinct potassium currents in the ventral cochlear nucleus,” *J. Neurophysiol.*, vol. 89, no. 6, pp. 3070–3082, Jun. 2003.
- [45] J. S. Rothman and P. B. Manis, “Kinetic analyses of three distinct potassium conductances in ventral cochlear nucleus neurons,” *J. Neurophysiol.*, vol. 89, no. 6, pp. 3083–3096, Jun. 2003.
- [46] M. H. Negm and I. C. Bruce, “Effects of I_h and I_{KLT} on the response of the auditory nerve to electrical stimulation in a stochastic Hodgkin-Huxley model,” in *Proc. 30th Annu. Int. Conf. IEEE Eng. Med. Biol. Soc.*, Aug. 2008, pp. 5539–5542.
- [47] I. Bruce and M. Negm, “ I_{KLT} and I_h may explain rapid and short-term spike-rate adaptation in auditory nerve fiber responses to cochlear implant stimulation,” in *Proc. 32nd ARO Midwinter Meet.*, Baltimore, MD, USA, Feb. 2009.
- [48] C. C. Chow and J. A. White, “Spontaneous action potentials due to channel fluctuations,” *Biophys. J.*, vol. 71, pp. 3013–3021, Dec. 1996.
- [49] H. Mino, J. T. Rubinstein, and J. A. White, “Comparison of algorithms for the simulation of action potentials with stochastic sodium channels,” *Ann. Biomed. Eng.*, vol. 30, no. 4, pp. 578–587, Apr. 2002.
- [50] I. C. Bruce, “Implementation issues in approximate methods for stochastic Hodgkin-Huxley models,” *Ann. Biomed. Eng.*, vol. 35, no. 2, pp. 315–318, Feb. 2007.
- [51] W. Nernst, “Zur Theorie des elektrischen Reizes,” *Pflügers Arch.*, vol. 122, no. 7–9, pp. 275–314, 1908.
- [52] A. V. Hill, “Excitation and accommodation in nerve,” *Proc. Roy. Soc. B*, vol. 119, pp. 305–355, 1936.
- [53] D. E. O’Gorman, J. A. White, and C. A. Shera, “Dynamical instability determines the effect of ongoing noise on neural firing,” *J. Assoc. Res. Otolaryngol.*, vol. 10, no. 2, pp. 251–267, Jun. 2009.
- [54] P. J. Drew and L. F. Abbott, “Models and properties of power-law adaptation in neural systems,” *J. Neurophysiol.*, vol. 96, no. 2, pp. 826–833, Aug. 2006.
- [55] M. S. A. Zilany, I. C. Bruce, P. C. Nelson, and L. H. Carney, “A phenomenological model of the synapse between the inner hair cell and auditory nerve: Long-term adaptation with power-law dynamics,” *J. Acoust. Soc. Am.*, vol. 126, no. 5, pp. 2390–2412, Nov. 2009.
- [56] M. S. A. Zilany, I. C. Bruce, and L. H. Carney, “Updated parameters and expanded simulation options for a model of the auditory periphery,” *J. Acoust. Soc. Amer.*, vol. 135, no. 1, pp. 283–286, Jan. 2014.
- [57] J. E. Smit, T. Hanekom, and J. J. Hanekom, “Predicting action potential characteristics of human auditory nerve fibres through modification of the Hodgkin-Huxley equations,” *S. Afr. J. Sci.*, vol. 104, no. 1, pp. 284–292, Jul./Aug. 2008.
- [58] J. E. Smit, T. Hanekom, and J. J. Hanekom, “Modelled temperature-dependent excitability behaviour of a single ranvier node for a human peripheral sensory nerve fibre,” *Biol. Cybern.*, vol. 100, no. 1, pp. 49–58, Jan. 2009.
- [59] J. E. Smit, T. Hanekom, A. van Wieringen, J. Wouters, and J. J. Hanekom, “Threshold predictions of different pulse shapes using a human auditory nerve fibre model containing persistent sodium and slow potassium currents,” *Hear. Res.*, vol. 269, no. 1–2, pp. 12–22, Oct. 2010.
- [60] J. J. Briare and J. H. M. Frijns, “The consequences of neural degeneration regarding optimal cochlear implant position in scala tympani: A model approach,” *Hear. Res.*, vol. 214, no. 1–2, pp. 17–27, Apr. 2006.
- [61] F. Rattay, T. Potrusil, C. Wenger, A. K. Wise, R. Glueckert, and A. Schrott-Fischer, “Impact of morphometry, myelination and synaptic current strength on spike conduction in human and cat spiral ganglion neurons,” *PLoS One*, vol. 8, no. 11, p. e79256, 2013.
- [62] W. A. Hossain, S. D. Antic, Y. Yang, M. N. Rasband, and D. K. Morest, “Where is the spike generator of the cochlear nerve? Voltage-gated sodium channels in the mouse cochlea,” *J. Neurosci.*, vol. 25, no. 29, pp. 6857–6868, Jul. 2005.



Mohamed H. Negm (S'06) was born in Giza, Egypt, in 1982. He received the B.Sc. degree (with Hons.) in biomedical engineering from Cairo University, Giza, in 2005. He then received the M.A.Sc. degree in biomedical engineering from McMaster University, Hamilton, ON, Canada in 2008. He is currently working toward the Ph.D. degree in the Computational Electromagnetics Laboratory, Electrical and Computer Engineering Department, McMaster University.

He was an Electronic Design Engineer in BMA for Design and Industry, Giza, Egypt, between 2005 and 2006. He joined the Electrical and Computer Engineering Department, McMaster University, in 2008. His research interests include antenna design for medical applications, optimization, embedded design, digital and analog electronics, and physiological modeling.

Mr. Negm has received the Ontario (OGS) and Ann Poucher Windsor Queen Elizabeth II graduate scholarships. He is an active volunteer with Let's Talk Science Canada.



Ian C. Bruce (S'96–M'98–SM'08) was born in Bendigo, Vic., Australia, in 1969. He received the B.E. (electrical and electronic) degree from The University of Melbourne, Melbourne, Vic., in 1991, and the Ph.D. degree from the Department of Otolaryngology, The University of Melbourne.

From 1993 to 1994, he was a Research and Teaching Assistant at the Department of Bioelectricity and Magnetism, Vienna University of Technology, Vienna, Austria. He was a Postdoctoral Research Fellow in the Department of Biomedical Engineering at

Johns Hopkins University, Baltimore, MD, USA, from 1998 to 2001. Since 2002, he has been with the Department of Electrical and Computer Engineering at McMaster University, Hamilton, ON, Canada, currently at the rank of Associate Professor. His research interests include auditory modeling, hearing aids, cochlear implants, tinnitus, neural coding of speech, digital speech processing, and stochastic processes. He is an Associate Editor of the *Journal of the Acoustical Society of America*.

Dr. Bruce is a Member of the Acoustical Society of America and the Association for Research in Otolaryngology and is a Registered Professional Engineering in Ontario.